Physics of the Earth and Planetary Interiors 354 (2024) 107227

Contents lists available at ScienceDirect

Physics of the Earth and Planetary Interiors

journal homepage: www.elsevier.com/locate/pepi

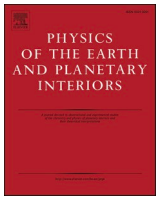

Simulation of microtextural evolution in omphacite: Ordering transformation kinetics as unexplored archives of slab eclogitization

Ryo Fukushima [a,*], Tatsuki Tsujimori [a,b], Nobuyoshi Miyajima [c]

[a] Graduate School of Science, Tohoku University, Sendai 980-8578, Japan
[b] Center for Northeast Asian Studies, Tohoku University, Sendai 980-8576, Japan
[c] Bayerisches Geoinstitut, Universität Bayreuth, 95440 Bayreuth, Germany

ARTICLE INFO

Keywords:
Omphacite
Ordering transformation
Antiphase domains (APDs)
Eclogite
Transmission electron microscopy (TEM)
Phase-field approach

ABSTRACT

Earth's subduction zone processes and surface environments are intricately governed by mass transfer phenomena at plate convergent boundaries. The determination of their rates and timings from high-pressure metamorphic rocks (e.g., eclogite), or remnants of ancient convergent boundaries, remains an ongoing challenge. Here, we proposed the potential and versatility of ordering transformation kinetics of omphacite, an essential mineral found in eclogite, as a dynamic recorder of the metamorphic history. Through macroscopic phase-field simulation, we explored the growth of antiphase domains (APDs) in metastable disordered omphacite, discussing the feasibility of constraining metamorphic reaction kinetics based on the size and morphology of omphacite APDs in eclogitized oceanic crust. Our simulation corroborated that omphacite nucleating later during the prograde metamorphism can exhibit an incompletely ordered state with sparsely distributed ordered domains, which suggests their usefulness in estimating the recrystallization timing of the omphacite. Additionally, we confirmed that the APD formation dynamics are significantly influenced by the initial cation configuration of the disordered matrix. This implies the APD morphology in natural omphacite under slab-surface conditions may reflect their precipitation kinetics. These findings provide valuable insights into the microtextural evolution of omphacite due to its ordering transformation, thereby enhancing our ability to interpret morphological features.

1. Introduction

Constraining the timings and rates of mass-transfer phenomena at Earth's plate convergent boundaries is of considerable importance to understand solid-earth processes and dynamic changes of surface environments. In addition to geophysical observations of modern subduction zones, traditional petrological approaches, combined with radiometric age dating of rocks that recrystallized at ancient plate boundaries, or high-pressure metamorphic rocks such as eclogite, have provided some constraints on such chemical geodynamics at convergent zones. However, there is an insurmountable barrier to the application of this traditional methodology, as the temporal resolution of the metamorphic mineral ages remains at $\sim 10^{5-6}$ years (e.g., porphyroblastic garnet; Pollington and Baxter, 2010; Gorce et al., 2021; Tual et al., 2022). This limitation may hinder the detection of their nucleation–growth timings, which are controlled by shorter-span fluid flushing or metasomatism (e.g., Yokoyama et al., 2002; Viete et al., 2018; Broadwell et al., 2019). Hence, there is an evident need to more precisely resolve the reaction kinetics and burial durations of the individual minerals.

To overcome this barrier, we revisited the ordering transformation kinetics of omphacite, a primary constituent of eclogite. Over the past half century, numerous studies have provided insights into the size, morphology and formation processes of antiphase domains (APDs) within omphacite—a microtexture formed by cation ordering (Champness, 1973; Phakey and Ghose, 1973; Carpenter, 1978, 1979a, 1979b, 1979c, 1982a, 1982b; Carpenter and Smith, 1981). The ordering, with a space group change from $C2/c$ to $P2/n$, is described by splitting of the individual M-cation sites, M1 for (Mg, Fe^{2+}, Al, Fe^{3+}) and M2 for (Na, Ca), into M1/M11 and M2/M21, respectively. Due to the breakdown of translational symmetry, antiphase boundaries (APBs) appear to form the APDs. Focusing on the aspects at which disordered omphacite first metastably appears, even at lower temperatures than the critical temperature of ~865 °C (Champness, 1973; Carpenter, 1978; Carpenter and Okay, 1978; Carpenter and Putnis, 1985) and at which APDs generally

* Corresponding author.
E-mail addresses: ryo.fukushima.p7@dc.tohoku.ac.jp (R. Fukushima), tatsukix@tohoku.ac.jp (T. Tsujimori), nobuyoshi.miyajima@uni-bayreuth.de (N. Miyajima).

https://doi.org/10.1016/j.pepi.2024.107227
Received 25 December 2023; Received in revised form 9 May 2024; Accepted 4 July 2024
Available online 9 July 2024

coarsen due to thermal annealing, Carpenter (1982b) proposed an empirical geothermometer/geospeedometer using the mean size of equiaxed APDs (δ), based on a positive correlation between APD sizes and peak metamorphic temperatures in natural omphacites:

$$\delta^8 = 8K_0 exp\left(-\frac{Q}{RT}\right)t, \quad (1)$$

where K_0 is a constant (6×10^{35} Å^8 yr^{-1}), Q is the activation energy ($3–4 \times 10^5$ J mol^{-1}), R is the gas constant, T is the annealing temperature, and t is the annealing time. Several researchers have discussed the peak metamorphic temperatures and metamorphic timescales of eclogites using this T–t–δ relationship (Lardeaux et al., 1986; Wu et al., 2000; Brenker et al., 2003; Müller et al., 2011; Pollok et al., 2014; Xie et al., 2020).

However, this T–t–δ relationship is, obviously, not precise enough to estimate detailed T–t paths, because this was only roughly calibrated so that mean equiaxed APD sizes in most of the observed samples were within a range of the geological timescale ($10^{4–8}$ years). In addition, we must reevaluate whether this relationship is truly applicable, especially for those formed at a depth of <~80 km along the typical subduction-zone thermal gradients (i.e., low-T eclogites: Tsujimori and Mattinson, 2021). Although Eq. 1 was established under the assumption that APD coarsening is solely driven by the reduction of the APB surface area, we have confirmed the presence of omphacite patches with heterogeneously bright ordered clusters (Fig. 1a) and with isolated ordered domains (Fig. 1b,c) in low-T eclogites (Fukushima et al., 2021b). For these textures, one cannot clearly define sharp APBs at least from the dark-field images, posing a question whether this assumption is valid in all cases. Besides, almost fully ordered omphacites (Fig. 1c,d) and those with a plenty of columnar APDs (Fig. 1c) sometimes coexist with such possibly metastable, disordered omphacites, leading to a difficulty in interpreting their formation histories. Strictly speaking, if incompletely ordered omphacites can remain in low-T eclogites, a simple application of the ripening theory without considering the incipient ordering stage could be insufficient to estimate the annealing timescale.

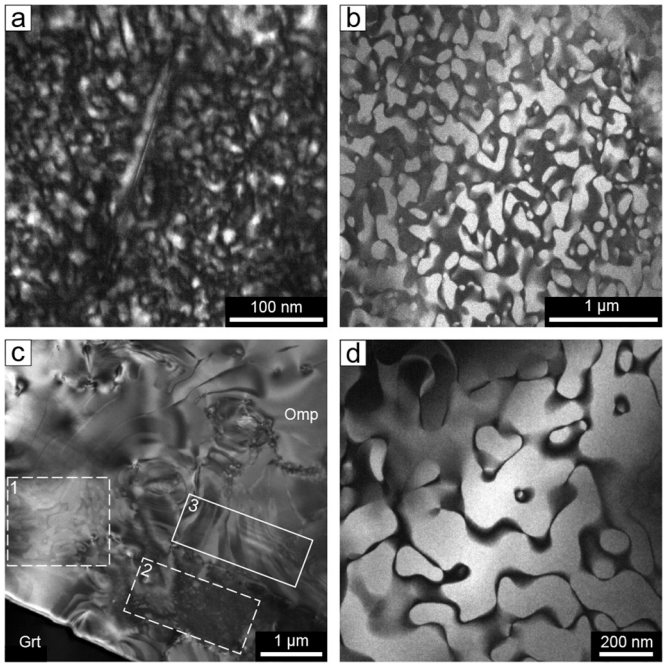

Fig. 1. Dark-field TEM images (g = 050) of natural omphacites from low-T eclogites. **a,** omphacite included in a garnet porphyroblast in a lawsonite eclogite from the South Motagua Mélange (SMM), Guatemala. X_{aeg} = 0.08; X_{aug} = 0.48; Mg# = 0.71; Fe^T = 0.23. **b,** omphacite with isolated equiaxed domains included in a garnet porphyroblast in an epidote-glaucophane eclogite from Syros, Greece (enlarged image of Fig. 6e in Fukushima et al., 2021b). The mean APD size (δ) and the ordered domain fraction (F) are ~100 nm and ~0.5, respectively. X_{aeg} = 0.00; X_{aug} = 0.47, Mg# = 0.66; Fe^T = 0.19. **c,** another omphacite inclusion with both equiaxed (dashed square) and columnar (solid square) APDs from the same garnet as **b**. Grt = garnet, Omp = omphacite. Representative compositions of the areas 1–3 are: X_{aeg} = 0.09, 0.24, 0.04; X_{aug} = 0.50, 0.48, 0.52; Mg# = 0.70, 0.62, 0.70; Fe^T = 0.25, 0.44, 0.21. **d,** typical equiaxed APDs in a matrix-forming omphacite in epidote eclogite from Omi, Japan. The mean APD size and the ordered domain fraction are ~140 nm and ~0.8, respectively. X_{aeg} = 0.02; X_{aug} = 0.54, Mg# = 0.77; Fe^T = 0.16.

Therefore, to establish a reasonable indicator of T–t histories based on the omphacite microtexture, we should first understand how cation ordering affects the final morphology of APDs, for a further calibration with natural samples. It may prove challenging to reproduce this cation ordering process with actual annealing experiments due to its sluggish kinetics (Carpenter, 1982b) and, as such, numerical simulation is the most effective way to understand the whole picture of the microtexture formation owing to cation ordering. To simulate the morphological changes of ordered domains, phase-field modeling has been widely used and recognized as a reliable approach in material science (e.g., Vaithyanathan and Chen, 2000; Zhu et al., 2004). This method basically requires the excess free energy function against one or several parameters to describe the local order-disorder state (and/or chemical compositions), as well as the other excess energy term(s) derived from the gradient of each parameter field. In the case of omphacite, Carpenter et al. (1990) proposed a tricritical Landau expansion for the excess free energy as a function of the order parameter, which can be directly incorporated into the phase-field model. Thus, the application of phase-field modeling to the omphacite system is a reasonable choice.

In this study, we use a phase-field approach to investigate how cation ordering affects the incipient APD formation in incompletely ordered omphacite. By leveraging a previously proposed expression of its excess free energy, we replicate the morphology and size of ordered domains in omphacite mainly under low-T eclogite-facies conditions. This is aimed at determining the feasibility of extracting relevant temporal information to constrain their nucleation timings from observable micro-to-nanoscale textures in natural omphacites.

2. Model setting

We adopted a macroscale, phenomenological phase-field model with a single order parameter for the omphacite M1 site, assuming that the ordering on the M2 site is linked to that on the M1 site (e.g., Ross, 1988; Carpenter et al., 1990). By solving a simple evolution equation with the previously proposed Landau expansion of the excess free energy in the isotropic system, we were able to simply examine how cation ordering proceeds in initially disordered omphacite with the ideal chemical composition in accordance with various input parameters. It is worth noting that the anisotropy of the gradient energy is disregarded here due to the rare occurrence of crystallographically oriented APBs in omphacite (Carpenter, 1979c). We also dismissed the presence of any compositional variation and lamellae within omphacite, and this allowed us to set the 4 principal parameters: (1) annealing temperature (T); (2) excess energy for sharp APBs (equilibrium APB energy); (3) the initial scalar field for the 'almost' disordered omphacite, which must be properly defined with some fluctuation for ordering to proceed; and (4) mobility (M) that relates real time (t) and normalized time for calculations (t^*) as $t^* = MRTt$. However, we further regarded the equilibrium APB energy, whose value is unknown for omphacite so far, as a constant for simplicity. This is because the possible temperature range for low-T eclogite formation is limited to ~450–600 °C, and because it might be affected by the compositional variation in such a narrow temperature range, as in the case of alloys (e.g., Yu et al., 1994; Gorbatov et al., 2016). Further model details and calculation procedures are described below.

2.1. Phase-field model

Owing to the simplification above, we can employ a general method for simulating the dynamics of the order-disorder phase transition with incipient ordering as in Ninomiya et al. (1990). Basically, our approach is the same as their method, except for the form of the excess free energy function. All the symbols are summarized in Table 1. We introduced a single phase-field parameter, $\phi(\boldsymbol{r}, t)$, whose value can range from −1 to +1. This parameter represents the degree of order for M1 sites (by its absolute value) and the relative phase (by its positive/negative sign) at a position $\boldsymbol{r}$ and time t. The total free energy of the system (G_{total}) is given by:

$$G_{\text{total}}[\phi(\boldsymbol{r}, t)] = \int_{\boldsymbol{r}} \frac{1}{v} \left\{ g_{\text{bulk}}(\phi, T) + \frac{a^2}{2} |\nabla \phi|^2 \right\} \mathrm{d}\boldsymbol{r}, \tag{2}$$

where v is a constant equivalent to the molar volume of omphacite (6.3295×10^{-5} m^3 mol^{-1}; the average of jadeite and diopside values (Holland and Powell, 2011)), $g_{\text{bulk}}(\phi, T)$ is the temperature-dependent bulk excess free energy of omphacite assuming a uniform degree of order (in J mol^{-1}), and a is a parameter that determines the isotropic gradient energy (in m J$^{0.5}$ mol$^{-0.5}$). The $g_{\text{bulk}}(\phi, T)$ is derived from the Landau-type expansion for omphacite whose composition is jd50 aug50 by Carpenter et al. (1990):

$$g_{\text{bulk}}(\phi, T) = 11.4(T - 1138)\phi^2 + 4317\phi^6, \tag{3}$$

where T is the annealed temperature in K. At a constant temperature, the minimum value of the $g_{\text{bulk}}(\phi, T)$ ($= -g_{\text{m}}$) can be achieved when $\phi = \pm \phi_{\text{m}} = \pm \sqrt[4]{\frac{22.8(1138-T)}{25902}}$, which correspond to the equilibrium states. As $\phi(\boldsymbol{r}, t)$ should be approximated as a non-conserved field (Carpenter and Salje, 1989), we considered the Allen-Cahn equation (Allen and Cahn, 1979):

$$\frac{\partial \phi}{\partial t} = -Mv \frac{\delta G_{\text{total}}}{\delta \phi}, \tag{4}$$

where M is the mobility in mol J^{-1} yr^{-1}. Dividing both sides by MRT, we obtained the evolution equation to be solved:

$$\frac{\partial \phi}{\partial t^*} = -\frac{1}{RT} \left\{ 22.8(T - 1138)\phi + 25902\phi^5 - a^2 \nabla^2 \phi \right\}, \tag{5}$$

where t^* is the normalized time defined as $t^* = MRTt$. Additionally, the isotropic gradient energy coefficient a was related to the APB energy (s in J m^{-2}) by considering the free energy of a flat interface between two fully ordered antiphase domains (Cahn and Hilliard, 1958):

$$s = \frac{\sqrt{2}a}{v} \int_{-\phi_{\text{m}}}^{\phi_{\text{m}}} \sqrt{g_{\text{bulk}}(\phi, T) + g_{\text{m}}}\, \mathrm{d}\phi. \tag{6}$$

Table 1
List of the symbols regarding the simulation.

symbol	description	input value
δ	mean equiaxed APD size	
R	gas constant	8.3143 J K^{-1} mol^{-1}
T	annealing temperature	400, 500, 550, 600 °C
t	time	
M	mobility	
t^*	normalized time	$MRTt$
F	ordered phase fraction	
σ	standard deviation of the initial fluctuation	10^{-2}, 10^{-4}, 10^{-6}, 10^{-8}, 10^{-10}
s	APB energy	0.50 J m^{-2}
ϕ	phase-field parameter	
G_{total}	total free energy of the system	See Eq. 2.
v	molar volume of omphacite	6.3295×10^{-5} m^3 mol^{-1}
a	isotropic gradient energy coefficient	Converted from s (Eq. 6.).
g_{bulk}	excess free energy of omphacite	See Eq. 3.
$-g_{\text{m}}$	minimum of the g_{bulk}	
ϕ_{m}	degree of order when $g_{bulk} = -g_m$	$(22.8\ (1138 - T)/25902)^{0.25}$
dx, dy, dz	grid size	5×10^{-9} m
dt	time step size	0.01

2.2. Calculation procedures

We basically conducted simulations in a 2-dimensional (2D) space with a 2 × 2 μm^2 area (400 × 400 grids) and employed periodic boundary conditions. Additionally, we attempted 3-dimensional (3D) simulations in smaller spaces (0.6 × 0.6 μm^2 area with 120 × 120 grids) to discuss the dimensional effects. The 3D results were compared with the 2D results by generating a 2D slice for each time step.

As the initial configurations, zero-mean Gaussian noise with a variance of σ^2 was independently introduced for each grid, each with a size of 5 nm on a side (dx, dy, dz). It is important to note that the grid size should be larger than the unit cell size to robustly define the macroscopic order parameter and the bulk free energy for each grid. In addition, we can assume that the approximate conservation length corresponds to the interatomic distance between neighboring crystallographic sites (~0.5 nm) (Carpenter and Salje, 1989). This suggests that the initial representative degree of order in a given grid should be independent of those in the adjacent grids. Therefore, to simplify matters, we discussed the initial cation configuration in terms of the fluctuation amplitude, based on the working hypothesis that the cation configuration of the metastable disordered omphacite can be essentially treated as the assembly of small portions with independent noise.

For the discretization of Eq. 5, we used a forward difference at time t^* and a second-order central difference for the space derivatives. The time-step size (dt) was fixed at 0.01 to ensure stable calculation results. The default value for the APB energy ($s = 0.50$ J m^{-2}) was determined so that simulation results at a temperature of 550 °C replicated the real equiaxed APD texture shown in Fig. 1b, assuming it is incompletely ordered. By tentatively setting the square root of the initial fluctuation variance as $\sigma = 10^{-4}$, we adjusted the s value to reproduce a mean APD size (δ) of ~100 nm when the ordered phase fraction (F) is ~0.5 in the 2D model. The order of magnitude of this s value, namely 10^{-1} J m^{-2}, is consistent with those of anorthite (Carpenter, 1994). For the dark-field-like image conversion, we assumed a response curve of the CCD camera with a certain saturation level (Supplementary Fig. S1), while ignoring completely buried ordered domains in the specimen. It is worth noting that we tentatively speculated a convex-upward function for slightly ordered states ($|\phi| < 0.1$) to replicate the contrast of the real dark-field images. For $|\phi| \geq 0.1$, where the sharp superlattice reflection due to the long-range order should be, at least, observed (Boffa-Ballaran et al., 1998), we used a convex-downward parabolic function, as implemented in the previous study (e.g., Ninomiya et al., 1990).

To quantitatively evaluate the individual snapshots of the evolving phase field, we calculated the mean degree of order (spatial average of $|\phi|$), the mean APD size (δ), the ordered phase fraction (F), and the spatial wavelength after every 50 time steps. For some representative cases, we also calculated histograms of $|\phi|$ to visualize the temporal change of its frequency distribution (i.e., 'power spectrum' as set forth in Salje and Wruck (1988)). Since the calculation of δ and F requires binarization of the corresponding phase field, we set a tentative threshold of $|\phi| = 0.4$ to convert it to a binarized image. The δ value was obtained by averaging all the ordered segment lengths along 50 nm-spacing lines. For the spatial wavelength calculation, we utilized a method for estimating the averaged grain size using the autocorrelogram of the sediment image (Buscombe et al., 2010). By calculating the autocorrelation of the phase field (before binarization) for each lag along one direction, we obtained its representative length scale.

All the simulations were implemented with a set of Python routines called Om-COS (Fukushima, 2023). We ran the scripts on the Windows 11 operating system using Python 3.9, with an AMD Ryzen™ 7 5700 G processor and 16 GB RAM.

3. Results

3.1. Advent and growth of ordered domains

The representative results of our modeling with random initial configuration are presented in Fig. 2a. It is clearly observed that partially ordered domains with various sizes randomly form in the almost disordered matrix and subsequently coarsen. At a later stage, the amplitude of the long-range order increases throughout the entire calculated area to form APBs with the equilibrium degree of order. This can be explained by the decreasing total contribution of the gradient energy term to suppressing ordering due to the slightly-ordered domain growth. By converting the order-parameter field into a corresponding gray-scale image, we reproduced images similar to the real dark-field images with abundant equiaxed APDs (Fig. 2b). It should be noted that only a ~50 °C difference of the annealed temperature leads to distinct textures in the ordered domain size; a slightly higher temperature can result in significantly larger, although fewer, domains.

The overall ordering process can be also figured out by generating a histogram for each representative time step (Fig. 3). The initial sharp distribution at $|\phi| = 0$ is broaden and extends to higher $|\phi|$ values, and finally produces a sharp peak again at the equilibrium degree of order. Even after the mode of the histogram (i.e., the most probable value) switches into around the equilibrium value, both the mean order parameter and the fraction of ordered domains continue increasing. As inferred from a previous theoretical study of disordering kinetics (Salje and Wruck, 1988), this could raise a difficulty in detecting any difference in 'transitional' omphacites (e.g., $t^* = 10.5$–12.5 in Fig. 3) only with conventional X-ray experiments, whose results would reflect the most probable state.

For the sensitivity analysis of each parameter, we summarized the time evolution of the spatially averaged order parameter (Fig. 4a), and the relationship between the mean APD size (δ) and the spatial fraction of the ordered phase (F) (Fig. 4b,c). Because the mobility (M) acts only as a scaling factor of time, in this study, we focus only on how the annealed temperature and the initial cation configuration influence the resultant texture. The degree of order was found to suddenly increase after a certain incubation period, and this depends on the magnitude of the initial fluctuation (Fig. 4a). Specifically, a larger initial variance (or a larger σ value) resulted in the incubation period being shorter at a constant temperature. Note that the temperature effect on the incubation duration is hard to evaluate since the mobility term should be a sensitive function of temperature. As to the δ–F relationship, both a higher temperature condition and a smaller initial variance lead to a

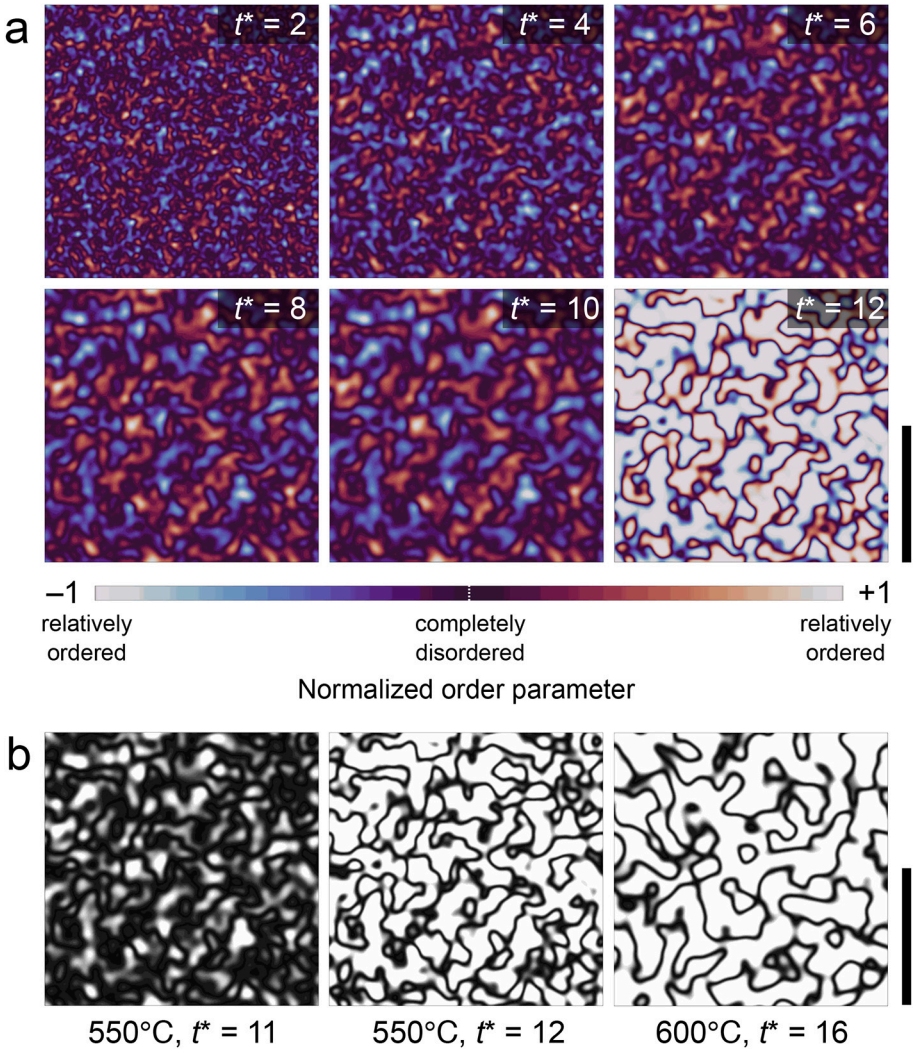

Fig. 2. Representative results of the 2D simulations of equiaxed APD formation (scale bar: 1 μm). **a,** the time evolution ($t^* = 2, 4, 6, 8, 10, 12$) of the phase field at a temperature of 550 °C. The positive/negative values of the phase field were plotted in reddish/bluish colors. For each snapshot, the field is normalized by the maximum degree of order. **b,** dark-field-image like visualization of selected results of the 2D simulations for equiaxed APD formation. Simulation results at 550 °C ($t^* = 11, 12$) and 600 °C ($t^* = 16$) are presented (brighter regions: ordered; darker regions: disordered). All the calculations were performed with $\sigma = 10^{-4}$.

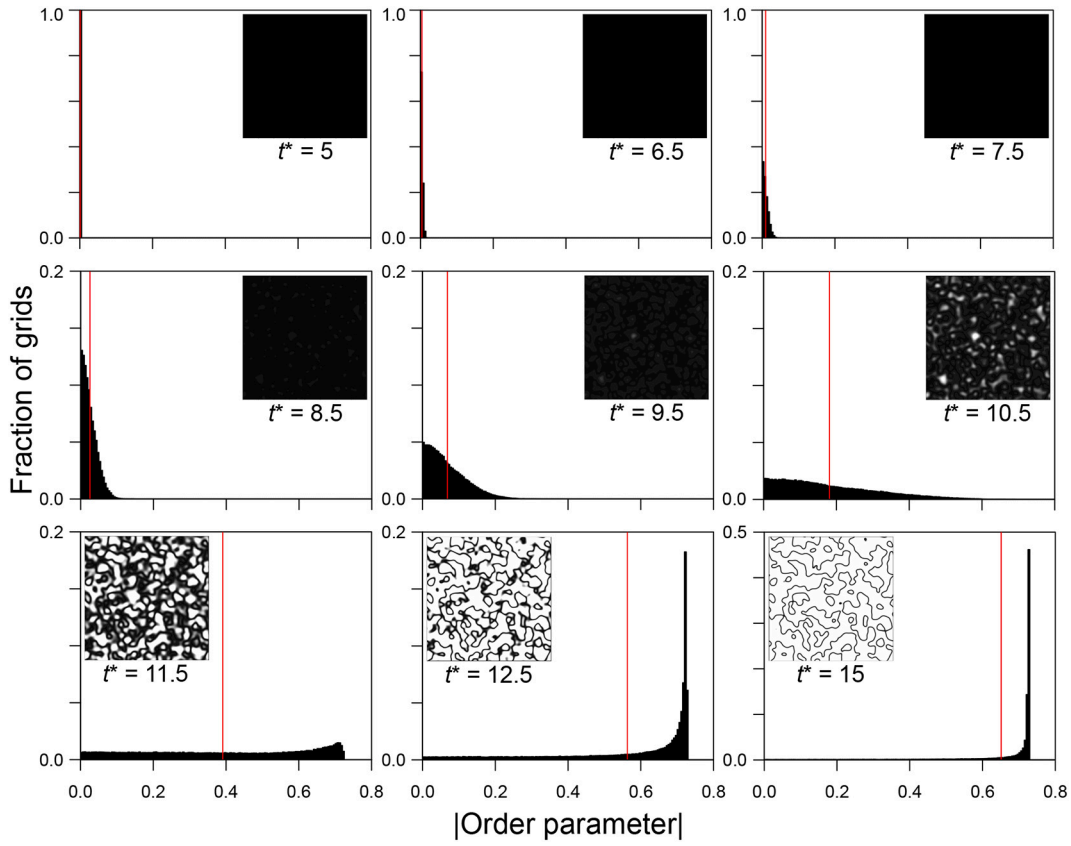

Fig. 3. Temporal evolution of the frequency distribution of the order parameter for a representative 2D simulation of equiaxed APD formation (550 °C, $\sigma = 10^{-4}$). The inset in each histogram ($t^* = 5$, 6.5, 7.5, 8.5, 9.5, 10.5, 11.5, 12.5, 15) shows the simulated dark field image (brighter regions: ordered; darker regions: disordered), and the red vertical line indicates the spatially averaged order parameter. The bin width of the histogram is set to 0.005. Note that the maximum value of the y-axis (fraction of grids in each class) is different: 1.0 or 100% ($t^* = 5$, 6.5, 7.5); 0.2 or 20% ($t^* = 8.5$, 9.5, 10.5, 11.5, 12.5); and 0.5 or 50% ($t^* = 15$). (For interpretation of the references to colour in this figure legend, the reader is referred to the web version of this article.)

larger δ/F ratio (Fig. 4b,c), which indicates the presence of larger but fewer ordered domains. A similar tendency was observed in the 3D simulation results (Supplementary Fig. S2), except that the incubation duration seems to be a little longer than that in the 2D case (Fig. 4a).

In addition, our quantification of their spatial wavelengths, which are naturally expected to be twice of the representative ordered cluster sizes, demonstrated that its growth would obey the parabolic rate law, regardless of the input parameters and the dimension (Fig. 4d). This is consistent with previous studies of the cluster size evolution during cation ordering in alloys (Hashimoto et al., 1978; Kawasaki et al., 1978). Note that we interpreted the wavelength drop shown in Fig. 4d (e.g., depicted by the yellow marker) as being caused by the abrupt ordering and subsequent topological changes in the phase field (cf., Marek and Demjen, 2017). We excluded the wavelength–time curves after such sudden decreases for the purpose of this research.

3.2. Interaction between equiaxed APDs and initial nuclei

Although our modeling with random initial configurations seems to replicate equiaxed APD textures in natural omphacites, this approach still cannot simulate microtextures with columnar APDs that terminate at grain boundaries and dislocations, as shown in Fig. 1c. There are two mechanisms proposed to explain such columnar APD growths: a heterogeneous nucleation process of ordered phases at a high supercooling degree (Champness, 1973; Carpenter, 1979c), and a rapid overgrowth of ordered omphacite grain (Fukushima et al., 2021b). However, the latter would be rare, and has been reported only in omphacites included in garnet porphyroblasts. Therefore, in this study, we attempted to model how columnar APDs grow from the initial ordered nuclei.

Because their heterogeneous nucleation processes cannot be technically simulated only with a simple phase-field approach, the columnar APD formation cannot be perfectly modeled unless the individual APD nucleation sites are successfully estimated. Here, we assumed that the initial presence of small completely ordered domains (randomly in-phase or antiphase to each other) were aligned along the bottom side of the simulation area. For the remaining area, we set random initial configurations, similar to those set in the previous case (See Supplementary Fig. S3 for the detailed model setup). This treatment serves to simplify the heterogeneous nucleation of the ordered domains as if they appeared immediately after the omphacite had recrystallized or precipitated. This approach also disregards the internal strain field and subsequent domain growth anisotropy, which would have influenced the resultant microtexture.

Our simulation revealed that the nuclei grow perpendicularly to the modeled nucleation boundary (or surface), making their shapes columnar, and finally interact with equiaxed ordered domains (Fig. 5a). On the beginning, the length of the columnar APDs monotonously increases. Thereafter, equiaxed ordered domains appear in the almost disordered matrix and each of them reaches the equilibrium degree of order, similar to the results observed in the previous modeling. After the pinning of the columnar APDs to the equiaxed ones, their elongation speed suddenly decreased, and the elongated domains subsequently shrunk due to domain coarsening. This suggests there should be a maximum elongation length for such columnar APDs that nucleated at grain boundaries or dislocations. Under a constant temperature, a smaller initial variance leads to larger maximum length, probably due to the longer incubation time for the equiaxed APD formation (Fig. 5b). Note that, depending on the amplitude of the initial fluctuation, ripening

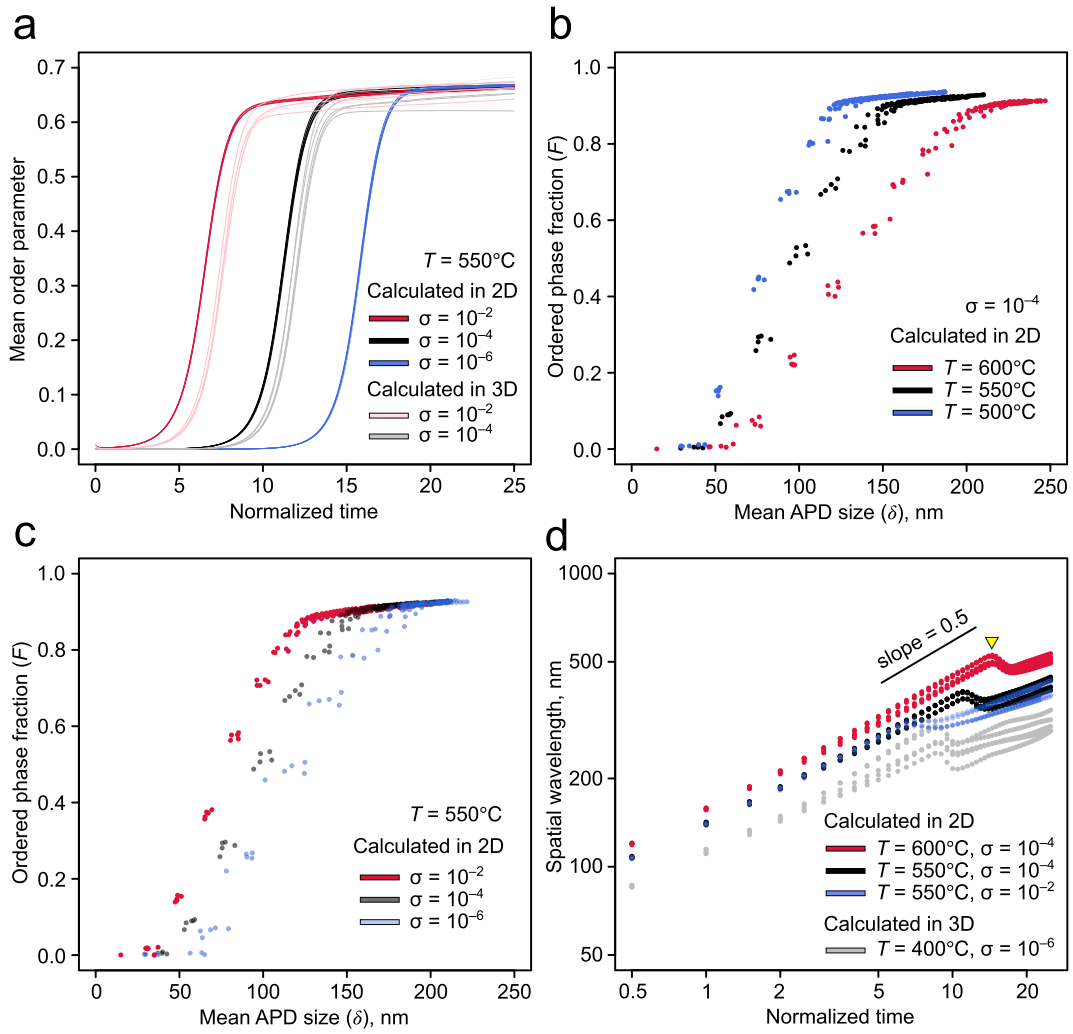

Fig. 4. Results of the sensitivity analysis of the input parameters (σ and T) for the equiaxed APD formation simulation. Under each condition, the simulation was performed 5 times to check the effects of the initial randomness. **a,** the time evolution of the spatially averaged order parameter with different σ values (10^{-6}, 10^{-4}, 10^{-2}) at 550 °C. Two representative results of the 3D simulations ($\sigma = 10^{-4}$, 10^{-2}) are also presented. **b,** the δ–F relationship at different temperatures (500, 550, 600 °C) with $\sigma = 10^{-4}$. **c,** the δ–F relationship with different σ values (10^{-6}, 10^{-4}, 10^{-2}) at 550 °C. **d,** the log–log plot of the spatial wavelength versus the normalized time with different conditions of (T, σ) = {(550 °C, 10^{-2}), (550 °C, 10^{-4}), (600 °C, 10^{-4})}. A 3D representative result with $T = 400$ °C and $\sigma = 10^{-6}$ is also presented. See details in the text for interpretation of the trends.

between the adjacent elongated domains can proceed before their impingement on the equiaxed APDs. The maximum length and the elongation speed of the columnar APDs with the corresponding parameters seems similar even in the 3D simulation, except that thinner columnar APDs diminish faster than in the corresponding 2D simulation (Supplementary Fig. S4).

4. Discussion

4.1. Dimensional effects

If we consider the larger measurement uncertainty of each parameter in the 3D simulation due to the smaller system size, we did not observe a significant difference between the 2D and 3D simulations in terms of the δ–F relationship, the growth exponent of ordered domains, and the maximum columnar APD length (or the elongation speed). On the other hand, domain coarsening between columnar APDs is faster, and the incubation time is slightly longer in the 3D simulation. We postulate that this is due to the larger gradient energy contribution for the individual ordered clusters or APDs in the 3D system. However, since our main focus is not the later-stage domain coarsening, and because this small difference in the incubation time can be compensated for by slightly adjusting the values of the initial fluctuation variance, the following discussion focuses on the incipient ordering process based on the 2D simulation results.

4.2. Timescale for the transitional state

Our simulation result of the equiaxed APD formation demonstrated that the duration of ordering from the initially disordered omphacite depends not only on the annealed temperature but also the initial cation configuration. The presence of an incubation period, probably due to the competition between the gradient and bulk energy terms, may allow the overall ordering rate to be slower than a simple assumption of uniform ordering would lead us to expect. Nevertheless, our simulation at a constant temperature suggests the timescale required for abrupt ordering is constant (e.g., ~5 normalized time units at 550 °C) regardless of the initial cation configuration (Fig. 4a).

Based on the observation that incompletely ordered omphacite with equiaxed APDs (δ ~100 nm, F ~0.5) remains in low-T eclogite from Syros, Greece (Fig. 1b), we can roughly estimate the duration required for the transition. Because the omphacite grain was included at the rim

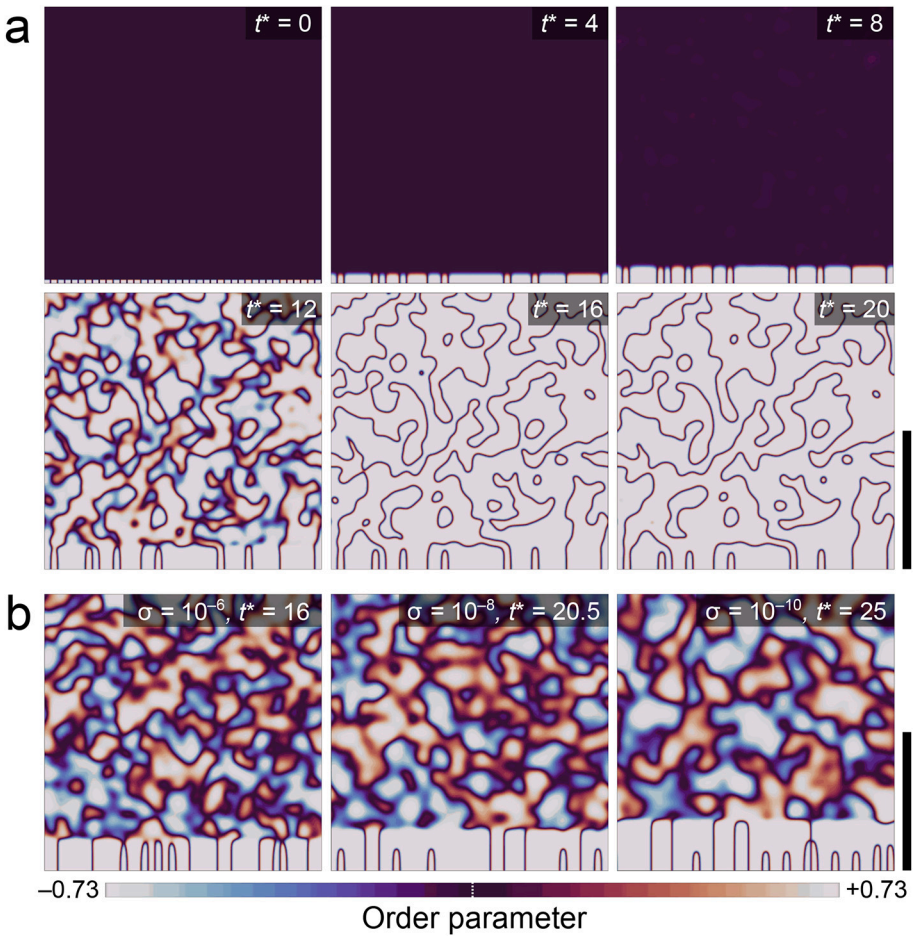

Fig. 5. Representative results of the 2D simulations of columnar APD formation (scale bar: 1 μm). **a,** the time evolution (t^* = 0, 4, 8, 12, 16, 20) of the phase field at a temperature of 550 °C and with σ = 10^{-4}. The maximum length of the columnar APDs is ~170 nm. **b,** selected results of the 2D simulations of columnar APD formation at 550 °C. Simulation results with σ = 10^{-6} (t^* = 16), σ = 10^{-8} (t^* = 20.5), and σ = 10^{-10} (t^* = 25) are presented. The maximum APD lengths are ~230 nm, ~300 nm, and ~370 nm, respectively.

of a garnet porphyroblast (Fukushima et al., 2021b), it should have been annealed at the peak metamorphic temperature of ~550 °C (Laurent et al., 2018) for a shorter time than the timescale of the whole eclogite-facies metamorphism. According to the previous geochronological studies of eclogite-facies rocks from the Cycladic Blueschist Unit (Lagos et al., 2007; Dragovic et al., 2012, 2015; Gorce et al., 2021; Tual et al., 2022), the age difference between the garnet-core formation and its post-peak isothermal decompression would be at most a few million years. Thus, we can, for example, envisage that the omphacite grain retained the incomplete order despite being annealed at 550 °C for 1 million years.

We found that the normalized time of t^* ~11.5 explains the microtexture with δ ~100 nm and F ~0.5 when σ = 10^{-4} (tentative, ~0.1% of the equilibrium value). Assuming t^* = 11.5 is equivalent to 10^6 years, the normalized time unit equals ~9 × 10^4 years, and the mobility (M) at 550 °C is calculated to be ~2 × 10^{-9} mol J^{-1} yr^{-1}. This subsequently means that the ordered-phase fraction rapidly increases within ~4 × 10^5 years (i.e., 5 normalized time units) at 550 °C. This order-of-magnitude estimate is consistent with the APD-size variation in a single natural low-T eclogite (Fukushima et al., 2021b); such a limited but not too-short timescale compared to the duration of isothermal decompression could allow for various APD textures depending on the timing of the individual omphacite crystallizations, especially in the later-stage eclogite-facies metamorphism. Thus, ordered domains in incompletely ordered omphacite could have the potential to record short-span events during slab eclogitization. Nevertheless, for a precise estimation of the mobility, we must choose the most feasible values for the model parameters, especially for the unknown initial fluctuation variance.

4.3. Assessment of the formation mechanism of columnar APDs

In our simulation of the columnar APD formation, their maximum lengths must be overestimated since fully ordered nuclei were introduced in the initial phase field. However, our simulation with various degrees of the initial fluctuation failed to reproduce longer columnar APDs than 1 μm (Fig. 5b), which were indeed observed in the natural omphacite specimens (Fig. 1c). Considering the incubation time mainly depends on the initial fluctuation variance and not much on any other parameters including the APB energy (Supplementary Fig. S5), this contradiction should be answered by the following two explanations about the initial configuration of the columnar-APD-rich omphacite: (1) the fluctuation was too small to simulate with our present model; or (2) the initial presence of heterogeneous, columnar domains that were already ordered to some extent (i.e., a non-random fluctuation in the initial disordered matrix).

If the first interpretation was correct, a question arises as to why the fluctuation is so small compared to equiaxed-APD-rich omphacites that escaped any heterogeneous nucleation of APDs along their grain boundaries/dislocations. Unfortunately, it is uncertain whether the initial fluctuation variance can be different by tens of order of magnitude between omphacites with equiaxed APDs and those with a plenty of

columnar APDs. On the other hand, the second explanation suggests that detailed microtextural analysis of columnar-APD-rich omphacites might be a key to estimating the initial cation configuration itself. For example, if a certain metastable disordered omphacite was formed by a dissolution–precipitation mechanism, such a local heterogeneity was likely to be introduced when the omphacite nucleated; and the crystal structure of parent minerals can remain in the newly-forming phases, possibly a silica-rich amorphous phase, to finally form the partially ordered omphacite (Hellmann et al., 2012; Konrad-Schmolke et al., 2018). Such a succession of the precursor structure is also inferred from the previous report of the irregular space group of omphacite replacing from igneous augite (Carpenter, 1978).

In any case, considering the microtextural variations (i.e., equiaxed and long columnar APDs) in natural omphacites included in the same garnet porphyroblast, we can conclude that there should have been some difference in the initial cation configuration among the individual metastable 'disordered' omphacites, even if they formed under similar *P*–*T* conditions. It should depend on its nucleation mechanism (e.g., direct nucleation from solute-bearing aqueous fluids, or recrystallization of lower-grade minerals such as chlorite and amphibole), and possibly the compositional heterogeneity of the precursors. This suggests an intimate relationship between the omphacite precipitation kinetics and its micron-scale ordered texture.

4.4. Constraints on the initial fluctuation amplitude

Our numerical simulation has revealed that cation configurations in the metastable disordered omphacite strongly affect the overall ordering rate and resultant APD textures. Given that disordered omphacite in natural low-*T* eclogites can nucleate via solid–solid reactions, and that its mineral reactants should be heterogeneously distributed on a micrometer scale, its metastable crystal structure should have been determined not only by temperature but also by bulk-rock chemical compositions, local chemical heterogeneity, and the precipitation kinetics of the omphacite grain. Considering these complex factors, it would be promising if one could determine the modeled initial fluctuation variance by analyzing the observed microtexture itself in a natural omphacite. Our simulation result of the equiaxed APD formation suggests that a two-order-of-magnitude difference in fluctuation standard deviation can be distinguished based on the observed domain size and fraction (Fig. 4c). Additionally, if there are any columnar APDs that nucleated at grain boundaries or dislocations in the early stage, we should be able to constrain the fluctuation amplitude from their maximum length (Fig. 5). In this sense, it may be possible to establish the initial fluctuation amplitude based on the natural microtextures, although the reliable calibration of all the other non-unique parameters, such as the APB energy, grid size, and ordered-phase threshold in the dark-field TEM images, would be still challenging.

4.5. Reliability of the excess free energy expression

In addition to the difficulty in calibrating the model parameters and estimating the initial cation configurations, we must carefully consider the reliability of the excess free energy expression of omphacite. The most questionable aspect of the Landau type expression is that the equilibrium degree of order at 500–600 °C (~0.69–0.75) is significantly lower than that of M1 sites (Q_{M1}) in some omphacites from natural low-*T* eclogites (~0.9). With the model we used here, such a highly ordered state can be attained at the equilibrium temperature of <200 °C. Although Carpenter et al. (1990) explained this as ordering occurring during cooling after peak metamorphism, there is no guarantee that ordering can proceed at such a low temperature. Indeed, a static energy calculation based on empirical interatomic potentials demonstrated the calculated equilibrium value of Q_{M1} at 600 °C is ~0.9 (Vinograd et al., 2007), suggesting a potential low-*T* inaccuracy in the model used in our simulation. There are, of course, alternative choices for free energy expressions, such as omphacite solid-solution models based on symmetric formalism (Holland and Powell, 1996; Green et al., 2007). Nevertheless, these models basically assume an identical value for the order parameters of M1 (Q_{M1}) and M2 (Q_{M2}) sites, oversimplifying the empirical correlation of $Q_{M1} = 2Q_{M2}$ (Carpenter et al., 1990; Boffa-Ballaran et al., 1998). Therefore, we need a more accurate expression for the omphacite free energy, especially at low-*T* eclogite-facies conditions.

Furthermore, when applying this model to natural omphacites, it is essential to consider the impact of compositional deviations on the bulk free energy (and potentially the gradient energy) as they are not negligible when discussing variations in ordered domain size and morphology. It is widely acknowledged that jadeite content influences the final APD size (Carpenter and Smith, 1981; Müller et al., 2011), and the addition of iron is known to suppress cation ordering (Cámara et al., 1998). Such deviated compositions lead to a reduction of the effective critical temperature, lowering the equilibrium degree of order, and making APBs thicker (Cahn and Hilliard, 1958). Thus, one should be cautious about discriminating incompletely ordered textures from equilibrium ones based only on the ordered domain fractions, without considering these effects.

For omphacite whose composition is extremely different from the ideal one, it is easy to judge that its microtexture is likely to be at equilibrium even though its ordered phase fraction is small. In fact, the area 2 omphacite in Fig. 1c is characterized by an extremely high iron content (See the caption and Supplementary Table S1), probably thereby tiny APDs are sparsely distributed there. However, for omphacite whose composition is relatively less deviated, the compositional criteria to assure incomplete ordering are still ambiguous. Further microtextural investigations combined with both precise compositional measurements and theoretical considerations are required.

4.6. Perspectives

Our simulation has revealed the versatility of incompletely ordered omphacite as a recorder of relatively short-span geodynamic histories and the precipitation kinetics of metastable disordered omphacite. Our results emphasize that the incipient ordering and later-stage domain coarsening should be treated as different regimes. This suggests that the previously proposed equation of $\delta^8 \propto t$ is not necessarily applicable to the low-*T* eclogite-facies omphacites. Even if such sluggish domain growth is due to impurity partitioning into the APBs (Carpenter, 1982b), its effects should be insignificant during the incipient ordering before the development of sharp APBs. Therefore, the mean size of ordered clusters in natural low-*T* eclogite-facies omphacites might follow the growth rate law $\delta^2 \propto t$ before reaching a completely ordered state (Fig. 4d). This time-sensitive domain growth would allow us to propose the potential of the microtexture in relatively young (i.e., later-nucleating) omphacites or incompletely ordered omphacites as a geo-speedometer. On the other hand, if certain metastable disordered omphacites are strongly characterized by the heterogeneous cation configurations and if later-stage domain coarsening is sluggish enough, the observable various APD morphologies may reflect different formation mechanisms of individual omphacite grains, rather than their burial durations.

Despite the invaluable insights of our simulations, we have encountered the limitation in the applications of such a simple forward modeling. We require reasonable calibration of the several parameters, including the initial cation configuration, the gradient energy, and the mobility values. To constrain the latter two variables, we might be able to perform experiments to observe the ordering process by using 'highly fluctuated' disordered omphacites. It has been reported that reordering of high-*T*-annealed omphacites occurred at 600 °C, probably due to the initial presence of short-range order (Holland, 1983). This suggests that a relatively large initial fluctuation enables such rapid ordering, as one can observe in a laboratory. Furthermore, we must consider that the limited number of APD observations, due to their time-consuming

procedures, may generally bias the characterization of a given eclogite. Both experiments and comprehensive analyses of natural omphacites are required for the further development of microtextural interpretation in omphacite.

If the ambiguity of the initial cation configuration and the imaging bias problem are solved, and if the compositional effect can be correctly handled, APD textures in omphacite would be a promising tool to constrain the kinetics of eclogite-facies slab dehydration. Specifically, its combined use with geochronology for eclogite-forming minerals (e.g., garnet, zircon) should open a new way for discussing short-span metamorphic events. Even if one has not calibrated the actual mobility value itself, the phase field model-based geospeedometer should enable its physically meaningful interpolation into a shorter timescale, based on a longer timescale constrained by the complement radiometric dating. In addition, one might be able to incorporate some effects of deformation and local strain, with the aid of TEM observations of various dislocations (e.g., Van Roermund and Lardeaux, 1991; Müller et al., 2011), lattice-preferred-orientation analyses for matrix-forming omphacites (e.g., Brenker et al., 2002; Urlich and Mainprice, 2005), and spectroscopic studies to measure residual stress in omphacite included in garnet (Baratelli et al., 2024). The establishment of the new indicator for the slab-eclogitization kinetics should help us understand the grain-scale reaction process, even from natural samples whose protoliths were totally replaced by the eclogitic mineral assemblages. Our investigation here is therefore the first step to realize this goal, by providing a cornerstone for disentangling its ordering transformation kinetics.

5. Conclusions

By revisiting microtextural formation processes due to the ordering transformation in omphacite under low-*T* eclogite-facies conditions, we demonstrate their potential for decoding the slab eclogitization kinetics. With the macroscopic phase-field approach, we can illustrate microtextural evolution due to cation ordering in a metastable disordered omphacite. Although it remains challenging to constrain the parameter values, our simulation suggests the size and fraction of ordered domains can significantly change within $<\sim 10^5$ years. In addition, our simulation results are consistent with the previous observation of various ordered-domain morphologies in natural omphacites under similar *P*–*T* conditions; there is no surprise if a given initial cation configuration determines the final microtexture, reflecting the nucleation–growth kinetics of the omphacite grain. This study proposes the new framework for analyzing omphacite microtextures, and would enlarge the applicability of their formation dynamics for petrogeological research of convergent orogens.

CRediT authorship contribution statement

Ryo Fukushima: Writing – review & editing, Writing – original draft, Visualization, Software, Project administration, Methodology, Investigation, Funding acquisition, Data curation, Conceptualization. **Tatsuki Tsujimori:** Writing – review & editing, Supervision, Resources, Funding acquisition, Conceptualization. **Nobuyoshi Miyajima:** Writing – review & editing, Investigation.

Declaration of competing interest

The authors declare no competing interests.

Data availability

Data will be made available on request.

Acknowledgments

This research received support from CNEAS at Tohoku University, BGI at the University of Bayreuth, and the Joint Usage/Research Center PRIUS, Ehime University, Japan (assisted by Hiroaki Ohfuji, Sayako Inoué, and Takeshi Sakai), and was funded in part by grants from the JSPS KAKENHI JP22KJ0304 to R.F. and JP21H01174 to T.T. The authors are also grateful to the International Joint Graduate Program in Earth and Environmental Sciences (GP-EES), Tohoku University. The Scios FIB and the Titan G2 TEM at BGI were financed by DFG Grant Nos. INST 91/315-1 FUGG and INST 91/251-1 FUGG, respectively. We express our deep appreciation to Mitsuhiro Toriumi and Tadao Nishiyama for their valuable comments on the simulation. We thank two anonymous reviewers for the constructive discussion, and Jie Li for her thoughtful editorial handling.

Appendix A. FIB-TEM/STEM-EDS analysis of natural omphacite specimens

We have selected natural omphacites from low-*T* eclogites in the SMM (Guatemala: Tsujimori et al., 2006), Syros (Greece: Fukushima et al., 2021b), and Omi (Japan) as representatives, as shown in Fig. 1. The omphacites from the SMM (one grain) and Syros (two grains) are found as inclusions in garnet porphyroblasts (Fukushima et al., 2021a), while the Omi omphacite (one grain) is a matrix-forming one. We prepared thin foils with a thickness of ~100–150 nm from each sample using the focused ion beam (FIB) technique. Subsequently, we captured dark-field TEM images of these foils using a transmission electron microscope. For the FIB fabrication process, we utilized the FEI Scios DualBeam FIB-SEM system, which is equipped with a gallium ion-gun and a thermal field emission electron gun, at Bayerisches Geoinstitut, Universität Bayreuth (BGI), and Geodynamics Research Center, Ehime University (GRC). The dark-field TEM images of the Syros omphacites were obtained using an FEI Titan G2 80–200 S/TEM at BGI, while those of the other omphacites were obtained using a JEOL JEM-2010 TEM at GRC.

Representative major element compositions of the individual samples were obtained by performing energy-dispersive X-ray spectroscopy (EDS) with 4 silicon drift detectors attached to the FEI Titan G2 80–200 S/TEM. The EDS spectra data were processed by using the software Esprit, with the Cliff-Lorimer method for the *Z*-number correction (Cliff and Lorimer, 1975) and the absorption correction based on experimentally calibrated k-factors of major elements including oxygen (van Cappellen and Doukhan, 1994). The ferric iron contents were estimated with $Fe^{3+} = Na - Al$, by speculating that Al is only located in the M1 sites. The site fractions of the other divalent cations were determined so that $(Ca + Mg + Fe^{2+})^{M2} = (Mg + Fe^{2+})^{M1}$ is maintained, assuming equipartition of Mg/Fe^{2+} between the M1 and M2 sites. We then calculated the following values to characterize each omphacite composition: $X_{aeg} = Fe^{3+}$, $X_{aug} = (Mg + Fe^{2+})^{M1}$, $Mg\# = [Mg/(Mg + Fe^{2+})]^{M1}$, and $Fe^{T} = (Fe^{2+} + Fe^{3+})$.

Appendix B. Supplementary data

Supplementary data to this article can be found online at https://doi.org/10.1016/j.pepi.2024.107227.

References

Allen, S.M., Cahn, J.W., 1979. A microscopic theory for antiphase boundary motion and its application to antiphase domain coarsening. Acta Metall. 27 (6), 1085–1095.

Baratelli, L., Murri, M., Alvaro, M., Prencipe, M., Mihailova, B., Cámara, F., 2024. Raman scattering of omphacite at high pressure: towards its possible application to elastic geothermobarometry. Am. Mineral. https://doi.org/10.2138/am-2023-9140.

Boffa-Ballaran, T., Carpenter, M.A., Domeneghetti, M.C., Tazzoli, V., 1998. Structural mechanisms of solid solution and cation ordering in augite-jadeite pyroxenes: I. A macroscopic perspective. Am. Mineral. 83 (5–6), 419–433.

Brenker, F.E., Prior, D.J., Müller, W.F., 2002. Cation ordering in omphacite and effect on deformation mechanism and lattice preferred orientation (LPO). J. Struct. Geol. 24 (12), 1991–2005.

Brenker, F.E., Müller, W.F., Brey, G.P., 2003. Variation of antiphase domain size in omphacite: a tool to determine the temperature–time history of eclogites revisited. Am. Mineral. 88 (8–9), 1300–1311.
Broadwell, K.S., Locatelli, M., Verlaguet, A., Agard, P., Caddick, M.J., 2019. Transient and periodic brittle deformation of eclogites during intermediate-depth subduction. Earth Planet. Sci. Lett. 521, 91–102.
Buscombe, D., Rubin, D.M., Warrick, J.A., 2010. A universal approximation of grain size from images of noncohesive sediment. Case Rep. Med. 115 (F2), F02015.
Cahn, J.W., Hilliard, J.E., 1958. Free energy of a nonuniform system. I. Interfacial free energy. J. Chem. Phys. 28 (2), 258.
Cámara, F., Nieto, F., Oberti, R., 1998. Effects of Fe^{2+} and Fe^{3+} contents on cation ordering in omphacite. Eur. J. Mineral. 10 (5), 889–906.
Carpenter, M.A., 1978. Kinetic control of ordering and exsolution in omphacite. Contrib. Mineral. Petrol. 67 (1), 17–24.
Carpenter, M.A., 1979a. Omphacites from Greece, Turkey, and Guatemala: composition limits of cation ordering. Am. Mineral. 64 (1–2), 102–108.
Carpenter, M.A., 1979b. Experimental coarsening of antiphase domains in a silicate mineral. Science 206 (4419), 681–683.
Carpenter, M.A., 1979c. Contrasting properties and behaviour of antiphase domains in pyroxenes. Phys. Chem. Miner. 5 (2), 119–131.
Carpenter, M.A., 1982a. Time-temperature-transformation (TTT) analysis of cation disordering in omphacite. Contrib. Mineral. Petrol. 78 (4), 433–440.
Carpenter, M.A., 1982b. Omphacite microstructures as time-temperature indicators of blueschist- and eclogite-facies metamorphism. Contrib. Mineral. Petrol. 78 (4), 441–451.
Carpenter, M.A., 1994. Evolution and properties of antiphase boundaries in silicate minerals. Ph. Transit. 48 (1–3), 189–199.
Carpenter, M.A., Okay, A., 1978. Topotactic replacement of augite by omphacite in a blueschist rock from north-west Turkey. Mineral. Mag. 42 (324), 435–438.
Carpenter, M.A., Putnis, A., 1985. Cation order and disorder during crystal growth: some implications for natural mineral assemblages. In: Thompson, A.B., Rubie, D.C. (Eds.), Metamorphic Reactions: Kinetics, Textures, and Deformation. Springer, New York, New York, pp. 1–26.
Carpenter, M.A., Salje, E., 1989. Time-dependent Landau theory for order/disorder processes in minerals. Mineral. Mag. 53 (372), 483–504.
Carpenter, M.A., Smith, D.C., 1981. Solid solution and cation ordering limits in high-temperature sodic pyroxenes from the Nybö eclogite pod, Norway. Mineral. Mag. 44 (333), 37–44.
Carpenter, M.A., Domeneghetti, M.C., Tazzoli, V., 1990. Application of Landau theory to cation ordering in omphacite I: equilibrium behaviour. Eur. J. Mineral. 2 (1), 7–18.
Champness, P.E., 1973. Speculation on an order-disorder transformation in omphacite. Am. Mineral. 58 (5–6), 540–542.
Cliff, G., Lorimer, G.W., 1975. The quantitative analysis of thin specimens. J. Microsc. 103 (2), 203–207.
Dragovic, B., Samanta, L.M., Baxter, E.F., Selverstone, J., 2012. Using garnet to constrain the duration and rate of water-releasing metamorphic reactions during subduction: an example from Sifnos, Greece. Chem. Geol. 314, 9–22.
Dragovic, B., Baxter, E.F., Caddick, M.J., 2015. Pulsed dehydration and garnet growth during subduction revealed by zoned garnet geochronology and thermodynamic modeling, Sifnos, Greece. Earth Planet. Sci. Lett. 413, 111–122.
Fukushima, R., 2023. Om-COS: cation ordering simulator for omphacite. Zenodo. https://doi.org/10.5281/zenodo.7982097.
Fukushima, R., Tsujimori, T., Aoki, S., Aoki, K., 2021a. Trace-element zoning patterns in porphyroblastic garnets in low-*T* eclogites: Parameter optimization of the diffusion-limited REE-uptake model. Isl. Arc. 30, e12394.
Fukushima, R., Tsujimori, T., Miyajima, N., 2021b. Various antiphase domains in garnet-hosted omphacite in low-temperature eclogite: a FIB-TEM study on heterogeneous ordering processes. Am. Mineral. 106 (10), 1596–1605.
Gorbatov, O.I., Lomaev, I.L., Gornostyrev, Y.N., Ruban, A.V., Furrer, D., Venkatesh, V., Novikov, D.L., Burlatsky, S.F., 2016. Effect of composition on antiphase boundary energy in Ni_3Al based alloys: *ab initio* calculations. Phys. Rev. B 93 (22), 224106.
Gorce, J.S., Caddick, M.J., Baxter, E.F., Dragovic, B., Schumacher, J.C., Bodnar, R.J., Kendall, J.F., 2021. Insight into the early exhumation of the Cycladic Blueschist unit, Syros, Greece: combined application of zoned garnet geochronology, thermodynamic modeling, and quartz elastic barometry. Geochem. Geophys. Geosyst. 22 (8), e2021GC009716.
Green, E., Holland, T., Powell, R., 2007. An order-disorder model for omphacitic pyroxenes in the system jadeite-diopside-hedenbergite-acmite, with applications to eclogitic rocks. Am. Mineral. 92 (7), 1181–1189.
Hashimoto, T., Nishimura, K., Takeuchi, Y., 1978. Dynamics on transitional ordering process in Cu_3Au alloy from disordered state to ordered state. J. Phys. Soc. Jpn. 45 (4), 1127–1135.
Hellmann, R., Wirth, R., Daval, D., Barnes, J.P., Penisson, J.M., Tisserand, D., Epicier, T., Florin, B., Hervig, R.L., 2012. Unifying natural and laboratory chemical weathering with interfacial dissolution–reprecipitation: a study based on the nanometer-scale chemistry of fluid–silicate interfaces. Chem. Geol. 294, 203–216.
Holland, T., 1983. The experimental determination of activities in disordered and short-range ordered jadeitic pyroxenes. Contrib. Mineral. Petrol. 82 (2–3), 214–220.
Holland, T., Powell, R., 1996. Thermodynamics of order-disorder in minerals: II. Symmetric formalism applied to solid solutions. Am. Mineral. 81 (11−12), 1425–1437.
Holland, T., Powell, R., 2011. An improved and extended internally consistent thermodynamic dataset for phases of petrological interest, involving a new equation of state for solids. J. Metamorph. Geol. 29 (3), 333–383.
Kawasaki, K., Yalabik, M.C., Gunton, J.D., 1978. Growth of fluctuations in quenched time-dependent Ginzburg-Landau model systems. Phys. Rev. A 17 (1), 455–470.
Konrad-Schmolke, M., Halama, R., Wirth, R., Thomen, A., Klitscher, N., Morales, L., Schreiber, A., Wilke, F.D.H., 2018. Mineral dissolution and reprecipitation mediated by an amorphous phase. Nat. Commun. 9 (1), 1637.
Lagos, M., Scherer, E.E., Tomaschek, F., Münker, C., Keiter, M., Berndt, J., Ballhaus, C., 2007. High precision Lu–Hf geochronology of Eocene eclogite-facies rocks from Syros, Cyclades, Greece. Chem. Geol. 243 (1–2), 16–35.
Lardeaux, J.M., Caron, J.M., Nisio, P., Péquignot, G., Boudeulle, M., 1986. Microstructural criteria for reliable thermometry in low-temperature eclogites. Lithos 19 (3–4), 187–203.
Laurent, V., Lanari, P., Naïr, I., Augier, R., Lahfid, A., Jolivet, L., 2018. Exhumation of eclogite and blueschist (Cyclades, Greece): pressure–temperature evolution determined by thermobarometry and garnet equilibrium modelling. J. Metamorph. Geol. 36 (6), 769–798.
Marek, J., Demjen, E., 2017. Is autocorrelation image analysis the proper method in nanoparticle sizing? J. Nanopart. Res. 19, 208.
Müller, W.F., Xu, Z., Brenker, F.E., 2011. Transmission electron microscopy of omphacite and other minerals in eclogites from the CCSD borehole, China: indications for their deformation and temperature history. Eur. J. Mineral. 23, 645–659.
Ninomiya, H., Eguchi, T., Kanemoto, H., 1990. Dynamics of pattern formation of antiphase ordered domain structures in alloys. Ph. Transit. 28 (1–4), 125–131.
Phakey, P.P., Ghose, S., 1973. Direct observation of anti-phase domain structure in omphacite. Contrib. Mineral. Petrol. 39 (3), 239–245.
Pollington, A.D., Baxter, E.F., 2010. High resolution Sm–Nd garnet geochronology reveals the uneven pace of tectonometamorphic processes. Earth Planet. Sci. Lett. 293 (1–2), 63–71.
Pollok, K., Heidelbach, F., John, T., Langenhorst, F., 2014. Spherulitic omphacite in pseudotachylytes: microstructures related to fast crystal growth from seismic melt at eclogite-facies conditions. Chem. Erde 74 (3), 407–418.
Ross, C.R., 1988. Statistical mechanical modeling of the kinetics of order-disorder in omphacitic pyroxenes. Phys. Chem. Miner. 15, 274–282.
Salje, E., Wruck, B., 1988. Kinetic rate laws as derived from order parameter theory II: interpretation of experimental data by Laplace-transformation, the relaxation spectrum, and kinetic gradient coupling between two order parameters. Phys. Chem. Miner. 16, 140–147.
Tsujimori, T., Mattinson, C., 2021. Eclogites in different tectonic settings. In: Elias, S., Alderton, D. (Eds.), Encyclopedia of Geology, 2nd ed. Academic Press, London, pp. 561–568.
Tsujimori, T., Sisson, V.B., Liou, J.G., Harlow, G.E., Sorensen, S.S., 2006. Petrologic characterization of Guatemalan lawsonite eclogite: Eclogitization of subducted oceanic crust in a cold subduction zone. Geol. Soc. Am. Spec. 403, 147–168.
Tual, L., Smit, M.A., Cutts, J., Kooijman, E., Kielman-Schmitt, M., Majka, J., Foulds, I., 2022. Rapid, paced metamorphism of blueschists (Syros, Greece) from laser-based zoned Lu-Hf garnet chronology and LA-ICPMS trace element mapping. Chem. Geol. 607, 121003.
Urlich, S., Mainprice, D., 2005. Does cation ordering in omphacite influence development of lattice-preferred orientation? J. Struct. Geol. 27 (3), 419–431.
Vaithyanathan, V., Chen, L.Q., 2000. Coarsening kinetics of δ′-Al_3Li precipitates: phase-field simulation in 2D and 3D. Scr. Mater. 42 (10), 967–973.
van Cappellen, E., Doukhan, J.C., 1994. Quantitative transmission X-ray microanalysis of ionic compounds. Ultramicroscopy 53 (4), 343–349.
van Roermund, H.L.M., Lardeaux, J.M., 1991. Modification of antiphase domain sizes in omphacite by dislocation glide and creep mechanisms and its petrological consequences. Mineral. Mag. 55 (380), 397–407.
Viete, D.R., Hacker, B.R., Allen, M.B., Seward, G.G.E., Tobin, M.J., Kelley, C.S., Cinque, G., Duckworth, A.R., 2018. Metamorphic records of multiple seismic cycles during subduction. Sci. Adv. 4 (3), eaaq0234.
Vinograd, V.L., Gale, J.D., Winkler, B., 2007. Thermodynamics of mixing in diopside–jadeite, $CaMgSi_2O_6$–$NaAlSi_2O_6$, solid solution from static lattice energy calculations. Phys. Chem. Miner. 34, 713–725.
Wu, X., Han, Y., Meng, D., Yang, W., Li, D., 2000. TEM and HRTEM study of microstructures in omphacite from UHP eclogites at Shima, Dabie mountains, China. Acta Geol. Sin. 74 (2), 154–162.
Xie, Z.J., Liu, X.W., Jin, Z.M., Li, Z.Y., 2020. Microstructures and phase transition in omphacite: constraints on the P-T path of Shuanghe eclogite (Dabie orogen). J. Earth Sci. 31, 254–261.
Yokoyama, T., Nakamura, E., Kobayashi, K., Kuritani, T., 2002. Timing and trigger of arc volcanism controlled by fluid flushing from subjecting slab. Proc. Jpn. Acad. Ser. B. 78 (7), 190–195.
Yu, H.F., Jones, I.P., Smallman, R.E., 1994. The effects of temperature, composition and strain rate on the deformation microstructure of Ni_3Al. Philos. Mag. A 70 (6), 951–967.
Zhu, J.Z., Wang, T., Ardell, A.J., Zhou, S.H., Liu, Z.K., Chen, L.Q., 2004. Three-dimensional phase-field simulations of coarsening kinetics of γ' particles in binary Ni–Al alloys. Acta Mater. 52 (9), 2837–2845.

Supplemental Material for:

Simulation of microtextural evolution in omphacite: Ordering transformation kinetics as unexplored archives of slab eclogitization

Ryo Fukushima[1], Tatsuki Tsujimori[1,2], and Nobuyoshi Miyajima[3]

[1]Graduate School of Science, Tohoku University, Sendai 980-8578, Japan

[2]Center for Northeast Asian Studies, Tohoku University, Sendai 980-8576, Japan

[3]Bayerisches Geoinstitut, Universität Bayreuth, 95440 Bayreuth, Germany

This file includes:

Figs. S1–S5 and Table S1

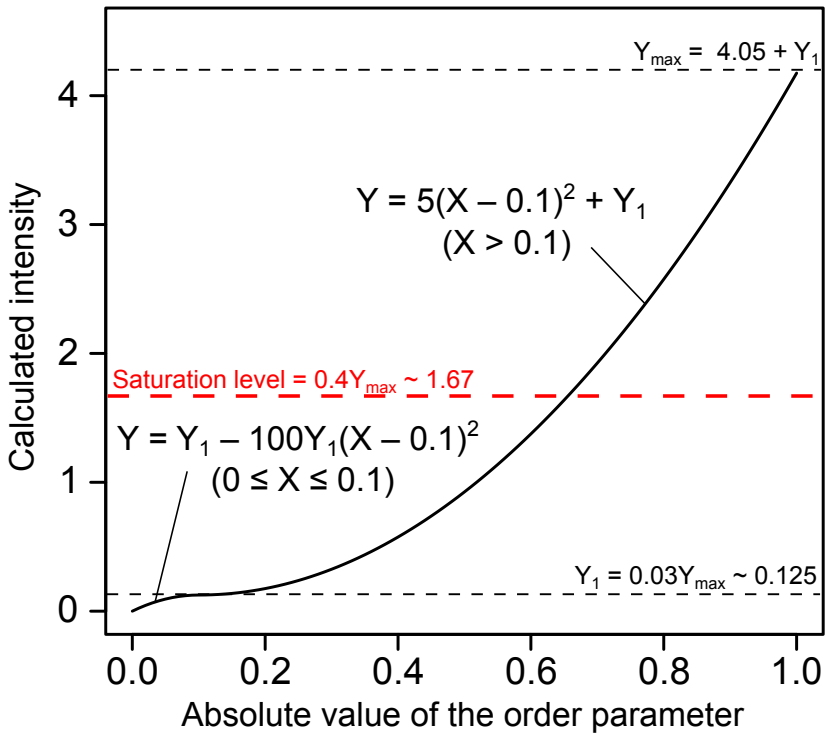

Fig. S1. The tentative response curve for the dark-field-like image conversion (black solid curve). Note that the saturation level (red dotted line) was set to 40% of the maximum intensity (Y_{max}).

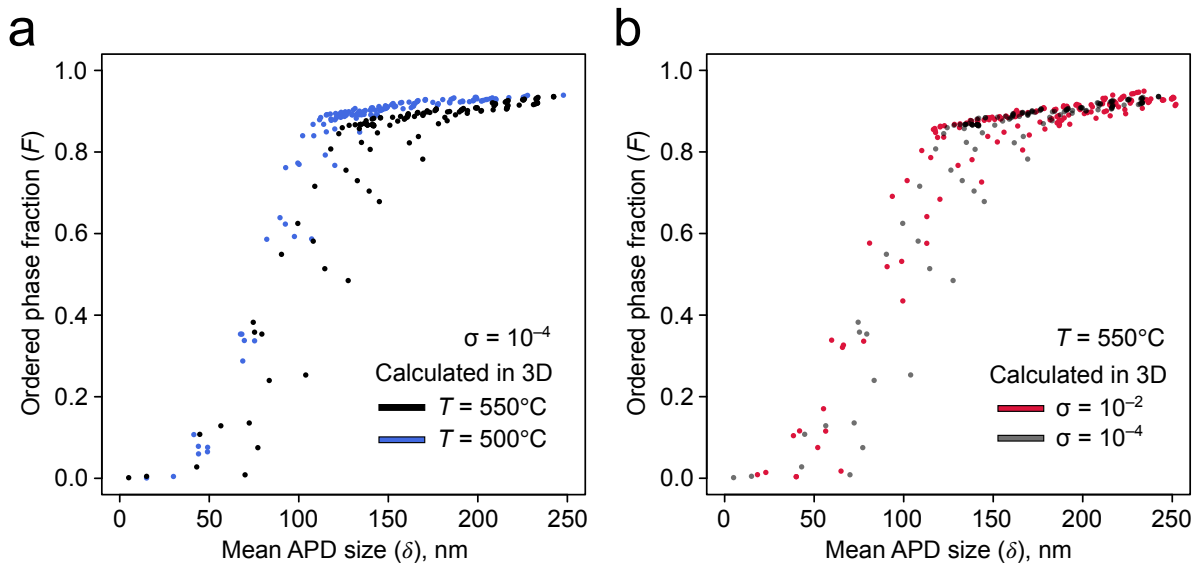

Fig. S2. Results of the sensitivity analysis of the input parameters (σ and *T*) for the equiaxed APD formation simulation in 3D systems. Each simulation was performed 5 times to check the effects of the initial randomness. **a,** the δ–F relationship at different temperatures (500 and 550°C) with $\sigma = 10^{-4}$. **b,** the δ–F relationship with different σ values (10^{-4} and 10^{-2}) at 550°C. Note that the 3D system size was smaller than that of 2D, which would have led to the large variations in the δ–F values.

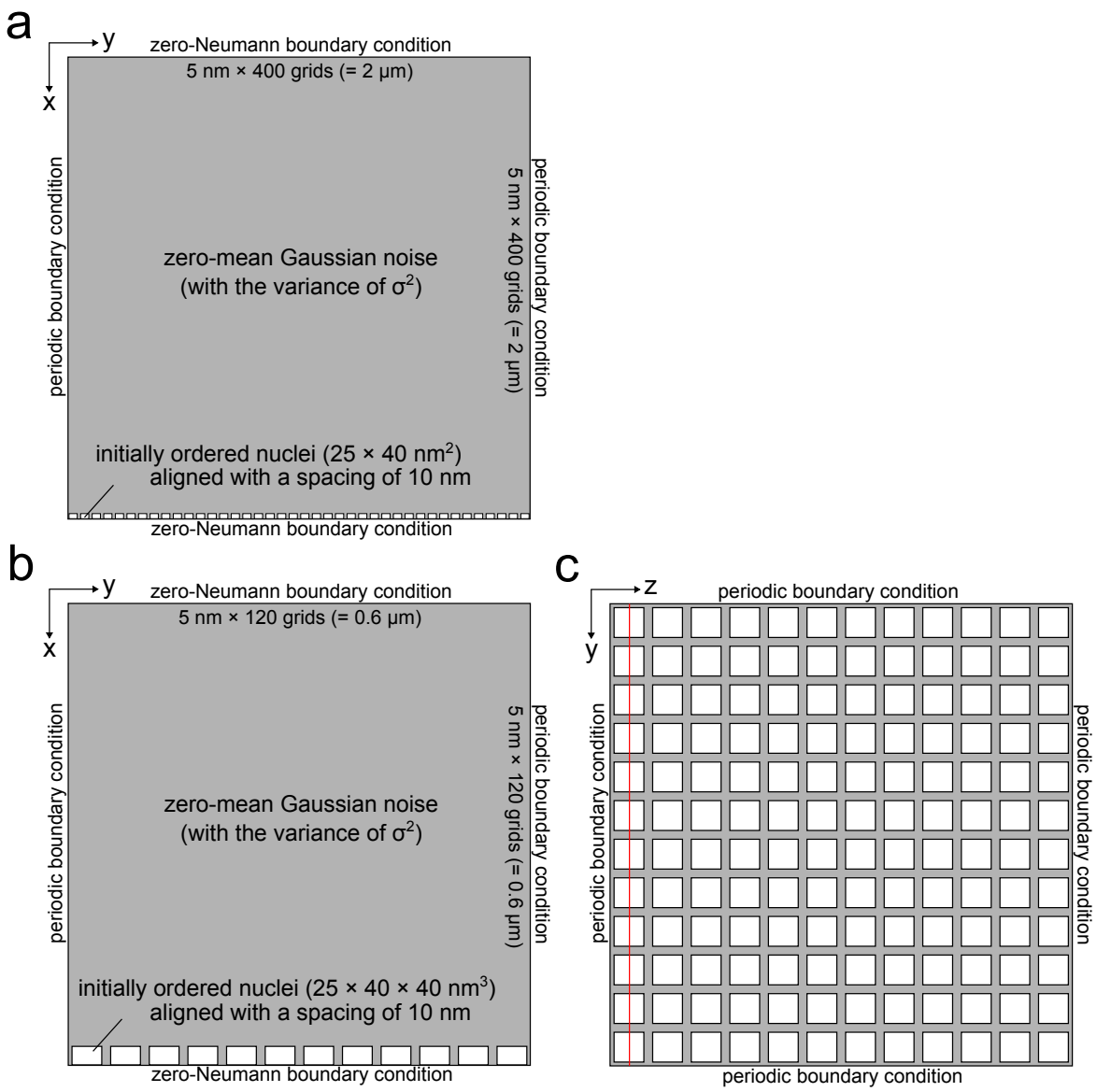

Fig. S3. Schematic figures showing the boundary conditions and initial configurations in the columnar APD simulations. The white rectangles/squares depict initially completely ordered nuclei, whose positive/negative signs were randomly designated. **a,** the condition in the 2D simulation. **b, c,** the condition in the 3D simulation on the z = 5 plane and x = 120 plane, respectively. The red line indicates the z = 5 plane.

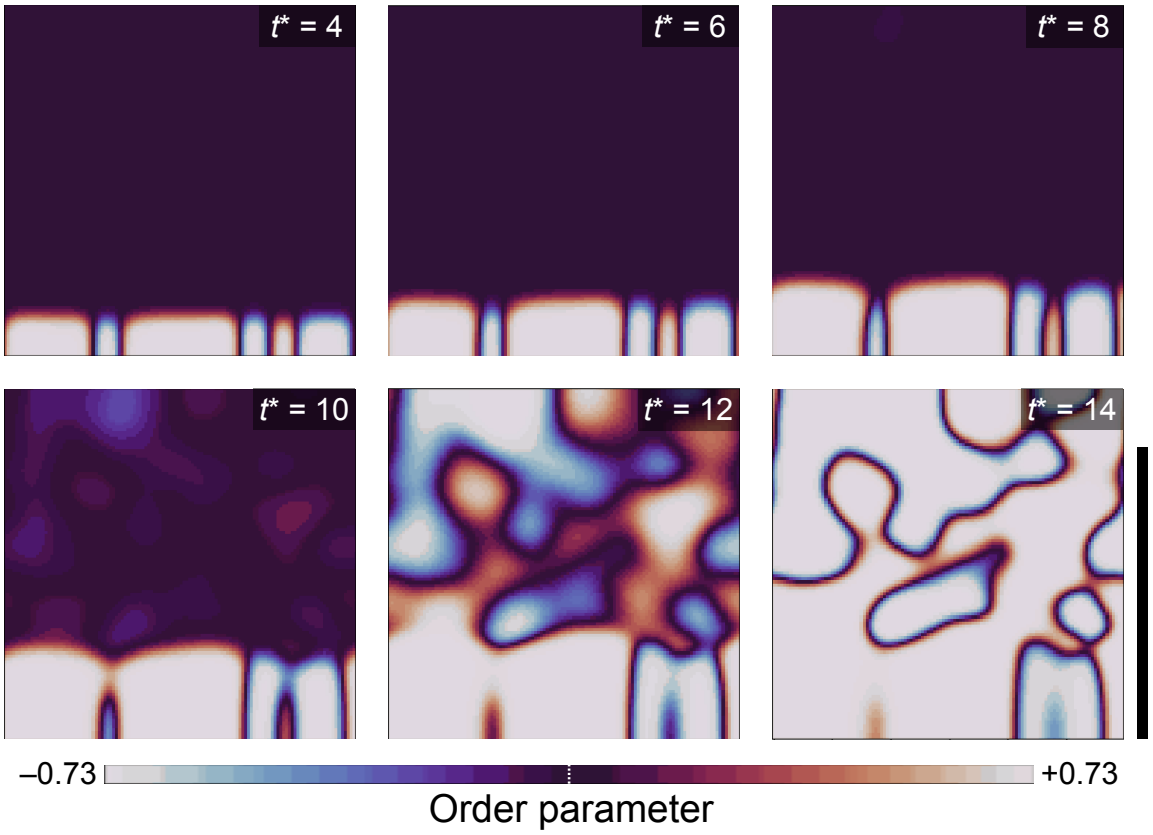

Fig. S4. A result of the 3D simulation of columnar APD formation (scale bar: 500 nm). The time evolution (t^* = 4, 6, 8, 10, 12, 14) of the phase field at a temperature of 550°C and with $\sigma = 10^{-4}$ is presented. The maximum length of the columnar APDs is ~170 nm, similar to the 2D simulation.

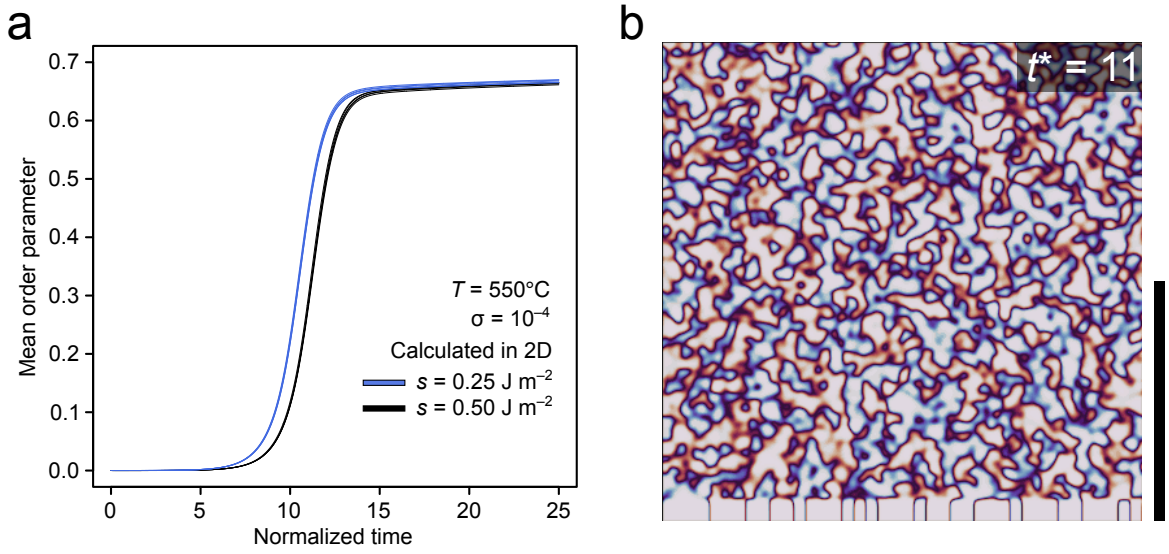

Fig. S5. Representative simulation results with a smaller APB energy value (s = 0.25 J m^{-2}, half of the default) in the 2D system (T = 550°C; σ = 10^{-4}). a, the time evolution of the spatially averaged order parameter (blue) in the equiaxed APD formation simulation. For comparison, the result with the default APB energy is also presented (black). Each simulation was performed 5 times to check the effects of the initial randomness. **b,** a snapshot of the columnar APD formation at a time of t^* = 11 (scale bar: 1 μm). The maximum APD length is ~100 nm, just ~60% of that in the default case, suggesting the difficulty in making long columnar APDs (e.g., 1 μm) with this order of magnitude (i.e., 10^{-1} J m^{-2}) of the APB energy value.

Table S1. Representative compositions of omphacites in Fig. 1 (O = 6).

	Fig. 1a (SMM)	Fig. 1b (Syros)	Fig. 1c-1 (Syros)	Fig. 1c-2 (Syros)	Fig. 1c-3 (Syros)	Fig. 1d (Omi)
$Si_{[T]}$	2.00	2.00	1.94	1.95	1.95	2.02
$Al_{[M1]}$	0.44	0.54	0.47	0.33	0.50	0.42
$Fe^{2+}_{[M1]}$	0.14	0.16	0.15	0.18	0.16	0.12
$Fe^{3+}_{[M1]}$	0.08	0.00	0.09	0.24	0.04	0.02
$Mg_{[M1]}$	0.34	0.31	0.35	0.30	0.36	0.42
$Fe^{2+}_{[M2]}$	0.01	0.03	0.01	0.02	0.01	0.02
$Mg_{[M2]}$	0.02	0.05	0.03	0.03	0.03	0.06
$Ca_{[M2]}$	0.45	0.39	0.47	0.43	0.48	0.46
$Na_{[M2]}$	0.51	0.52	0.56	0.57	0.54	0.44
Total	4.00	3.99	4.06	4.05	4.05	3.98